Application of Magnetic Multiple Resonance Techniques to the Study of Point Defects in Solids

J.-M. Spaeth

University of Paderborn, Fachbereich Physik, Warburger Str. 100 A, 4790, Paderborn, Federal Republic of Germany

Abstract

The determination of the microscopic structure of point defects in insulating and semi-conducting solids is based on the analysis of hyperfine and superhyperfine interactions. Usually the latter can only be measured by performing electron-nuclear double resonance (ENDOR) experiments. Recent developments of ENDOR spectroscopy, which are based on computer-aided experiments and analysis of spectra, are reviewed and illustrated with some examples. With these techniques and with advanced methods like ENDOR-induced EPR and DOUBLE ENDOR, complex defect problems arising in materials science can be solved. Recently, the optical detection of EPR and ENDOR (ODEPR, ODENDOR) via the optical absorption of defects was successfully applied to the study of defects in insulators and semiconductors. With an excitation spectroscopy of ODEPR and ODENDOR lines, direct correlation between optical bands and EPR/ENDOR lines of a particular defect becomes possible. By photo-ODEPR/ODENDOR techniques in semi-conductors, in which paramagnetic species are formed by exciting electrons from the valence band into upper levels, the energy level position of the defects within the gap could be determined. Examples are given to illustrate these optical techniques.

1. Introduction

The microscopic identification of point defects in non-metallic solids is a continuing problem in solid state physics. There is a renewed and vital interest in this kind of investigation coming from materials science, since point defects very often predominantly determine the bulk properties of solids. The search for tunable solid state lasers and semiconductor physics are just two specific areas where the understanding of point defects is of vital interest. For example, the Fermi level can be shifted within the band gap, utilizing specific doping, such that the defects of interest (*e.g.*, intrinsic defects) can be produced in a

Electronic Magnetic Resonance of the Solid State
Edited by John A. Weil (Associate editors: Michael K. Bowman, John R. Morton, Keith F. Preston).
Published by The Canadian Society for Chemistry, Ottawa, Canada 1987
ISBN: 0-921763-00-X

paramagnetic charge state.

In this article, recent developments of the application of magnetic multiple resonance techniques to the study of point defects in ionic and semiconductor crystals will be briefly reviewed.

The determination of the defect structure is based on the measurement of hyperfine (hf) interactions. It is useful to distinguish between the 'hf' interaction with a central nucleus, which might be there in the case of an impurity defect, and the superhyperfine (shf) [or ligand hyperfine] interactions, which are those with nuclei of the surrounding crystalline environment. The hf interaction can mostly be resolved by electron paramagnetic resonance (EPR), while for the resolution of shf interactions in general, electron nuclear double resonance (ENDOR) experiments are required. Although the latter technique was introduced over 27 years ago by G. Feher (1), its application remained restricted to comparatively few 'model' defects such as color centers in alkali halides. The reason may have been that the ENDOR spectra easily get very complicated, *e.g.*, if there are many neighbor nuclei interacting and/or if the defects (and host crystal) are of low symmetry. Considerable progress has been made in recent years by introducing computer-aided methods both in the experiment and the analysis of spectra and by introducing advanced ENDOR techniques. Some aspects of this will be reviewed with the emphasis on its use to characterise defects for materials science.

Optical detection of magnetic resonance has also been known for many years and can be done with several methods. It is a standard technique in the study of organic crystals, using the properties of excited triplet states. In ionic crystals and semiconductors the potentially high sensitivity and the possibility of studying excited states are of particular interest. Optical detection of EPR in the donor-acceptor recombination luminescence has become a standard tool in semiconductor physics (for a review see, *e.g.*, (2)). However, due to exchange interactions between donors and acceptors the spectra frequently do not show resolved hf interactions, which makes a defect identification often impossible. Recently, another technique of optical detection which was originally used to study the relaxed excited states of color centers in alkali halides (3), has proved very useful for defect characterization. Here EPR is detected by measuring the microwave-induced change of the magnetic circular dichroism (MCD) of the optical absorption. It will be reviewed how the latter technique can be used to selectively study defects with high sensitivity, to correlate optical bands with EPR spectra, to determine energy levels of defects, and to measure ENDOR in which shf-interactions are resolved.

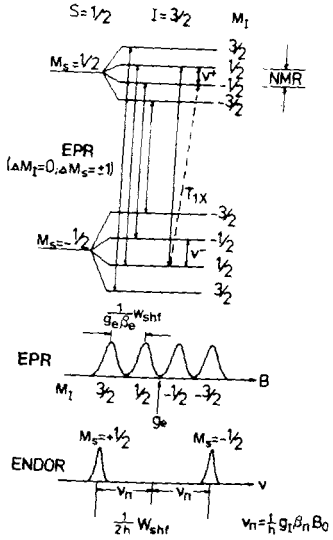

Figure 1. Schematic representation of stationary ENDOR for the simplified system of $S = 1/2$ having a hyperfine interaction with one nucleus with $I = 3/2$.

2. Electron Nuclear Double Resonance (ENDOR)

In ENDOR the nuclear magnetic resonance (NMR) transitions of nuclei coupled to the unpaired electron of the defect are observed by monitoring the increase of the partially saturated EPR signal upon fulfilling the double resonance condition. The method is illustrated schematically in Figure 1 for $S = 1/2$ and one nucleus with $I = 3/2$. Saturation is achieved if the EPR transition probability $w_{MW} \propto (g \beta_e B_1)^2$ is of the order of or larger than the spin-lattice relaxation rate $w_{REL} \propto 1/T_1$ (β_e is the Bohr magneton, B_1 the excitation (microwave) field amplitude, T_1 the electron spin lattice relaxation time). This usually implies low temperature, typically between 4 and 50 K. In most solids the cross-relaxation characterised by T_{1X} in Figure 1 is operating well enough to allow ENDOR to be observed as a stationary effect (4). Only stationary ENDOR will be discussed here. Usually the ENDOR effect is rather small, at most 1–2% of the EPR signal, but often much smaller. Therefore, a rather high number of defects and a highly sensitive spectrometer at low rf modulation frequencies is required. Superheterodyne spectrometers often are rather complicated. The availability of low-noise microwave amplifiers has made it possible to work with homodyne spectrometers (5).

The spin-Hamiltonian describing a defect having one unpaired electron, an

isotropic g-factor, as well as superhyperfine (shf) and nuclear quadrupole interactions is

$$[1] \qquad \mathcal{H} = g\beta_e \vec{S}^T \cdot \vec{B}_0 + \sum_l (\vec{S}^T \cdot \bar{A}_l \cdot \vec{I}_l - g_l \beta_n \vec{I}_l^T \cdot \vec{B}_0 + \vec{I}_l^T \cdot \bar{P}_l \cdot \vec{I}_l)$$

The sum runs over all nuclei interacting with the unpaired electron(s). The symbols have their usual meaning (6). In perturbation theory of first order, that is, with the condition that the anisotropic shf constant b and the nuclear quadrupole constant q are small compared to the isotropic shf constant a and the nuclear Larmor frequency, respectively, the ENDOR frequencies are (4)

$$[2] \qquad \nu_{\text{ENDOR}}^{\pm} = |M_S W_{\text{shf}} \mp g_l \beta_n B_0 \pm M_q W_Q| \frac{1}{h}$$

with

$$[3] \qquad W_{\text{shf}} = a + b(3\cos^2\theta - 1) + b' \sin^2\theta \cos^2\delta$$

$$[4] \qquad W_Q = 3\{q(3\cos^2\theta' - 1) + q' \sin^2\theta' \cos^2\delta'\};$$

θ, δ and θ', δ' are the polar and azimuthal angles of $\vec{B}_0$ in the principal shf and quadrupole axis systems, respectively. Here

$$[5] \qquad M_q = \frac{M_l + M_{l'}}{2},$$

where M_q is the average of the two nuclear spin quantum numbers connected by the transition.

Each nucleus interacting gives rise to 2 ENDOR frequencies in the absence of quadrupole interaction, and to 2×2 lines with quadrupole interaction for $S = 1/2$. In order to determine the orientations and principal values of the shf and quadrupole matrices, the ENDOR spectra have to be measured as a function of crystal orientation with respect to the static magnetic field B_0. The analysis of this ENDOR angular dependence is the basis for the structure determination of the defects (4, 7). For each crystal orientation, several hundred ENDOR lines can occur (*e.g.*, for Ni^{3+} in GaP over 600 lines (8)), which makes both experiment and analysis unfeasible unless computer-aided methods are applied. In the spectrometers of the Paderborn group, the computer controls the rf (NMR) frequencies, static magnetic field, crystal orientation, sample temperature and resonator matching. The ENDOR angular dependence can be measured automatically in small angular steps. A full angular dependence can take up to 2–3 weeks of continuous measurement. The frequency positions of the ENDOR lines are determined by applying a particular

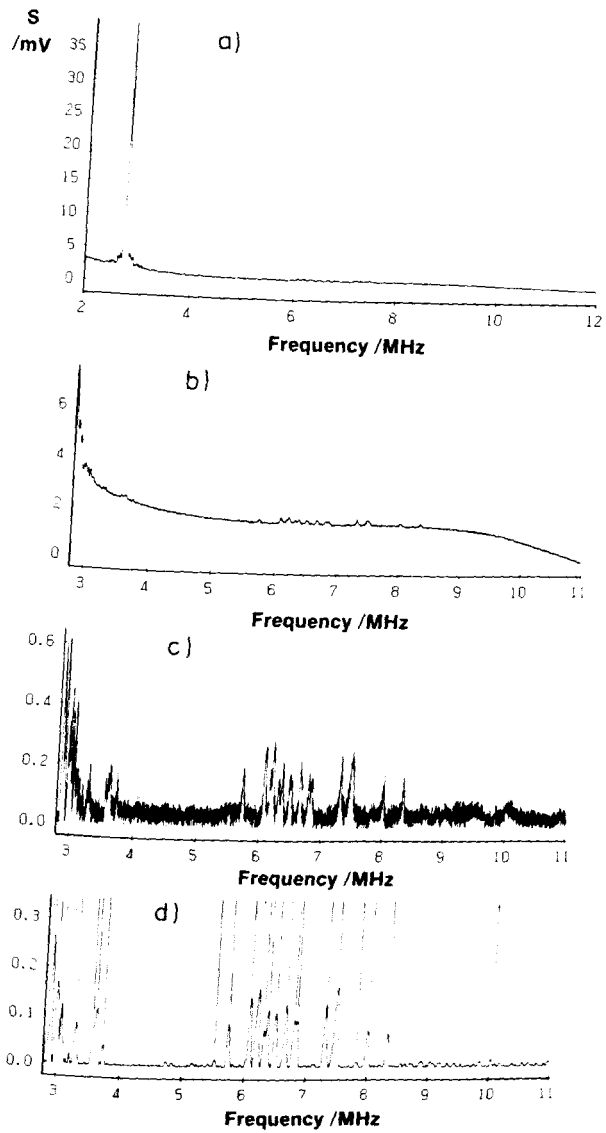

Figure 2. Digital signal processing for the example of interstitial Fe^0 centres in Si. (a) Stationary ENDOR as measured at X-band, 20 K, B_0 = 327.73 mT and approximately 20° off the [100] direction in a (110) plane. The lines of interest are those between 5 and 9 MHz. (b) After subtraction of the strong ^{29}Si "distant" ENDOR. (c) After subtraction of the strong background. (d) After digital filtering and "peak searching". The vertical lines mark the ENDOR line frequencies. (After 14).

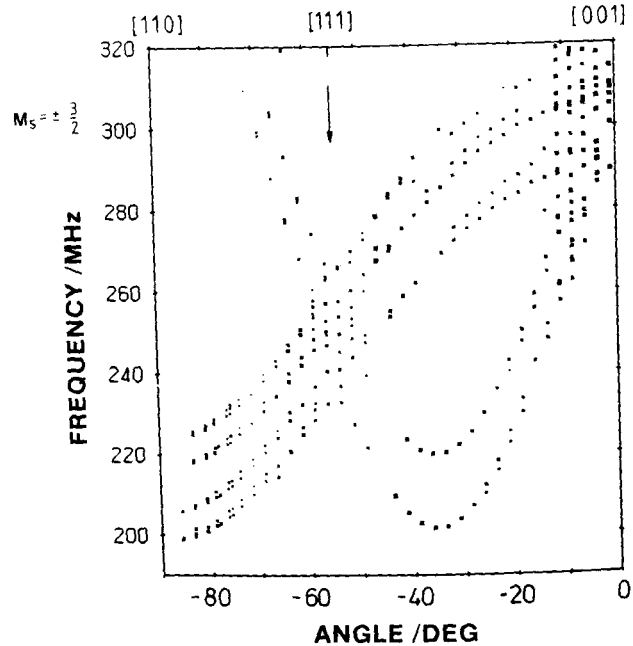

Figure 3. Angular dependence of the ENDOR signals from ^{31}P ($I = 1/2$) nearest-neighbor nuclei of the Ga vacancy in GaP under rotation of $\hat{B}_0$ in a (110) plane; $S = 3/2$. T = 6 K, X-band.

'peak search' algorithm (9). Before this can be done, usually digital filtering is applied (10–14). The digital filters conserve the first and second moments of the lines. In some cases a background is subtracted with a special algorithm (9). Often deconvolution procedures are needed when too many ENDOR lines overlap (9). Figure 2 illustrates the results of the application of such digital methods to the processing of the experimental data for the example of interstitial Fe^0 centers in Si (14). Figure 3 shows the angular dependence of nearest-neighbor ^{31}P ENDOR lines of the Ga-vacancy in GaP ($S = 3/2$). The dots represent the ENDOR frequencies, their size giving a measure of the line intensities (15). The Ga-vacancy was expected to have a perfect T_d symmetry for which, according to equation [2], for each orientation only 3 ENDOR lines for each M_S were expected for $\hat{B}_0$ in a (110) plane in contrast to the observation. The question was whether the multiplicity of lines is due to a superposition of several slightly distorted defects (the vacancy was produced by electron irradiation) or whether all lines belong to one defect. This can be determined by DOUBLE ENDOR. Two NMR frequencies are applied simultaneously, to-

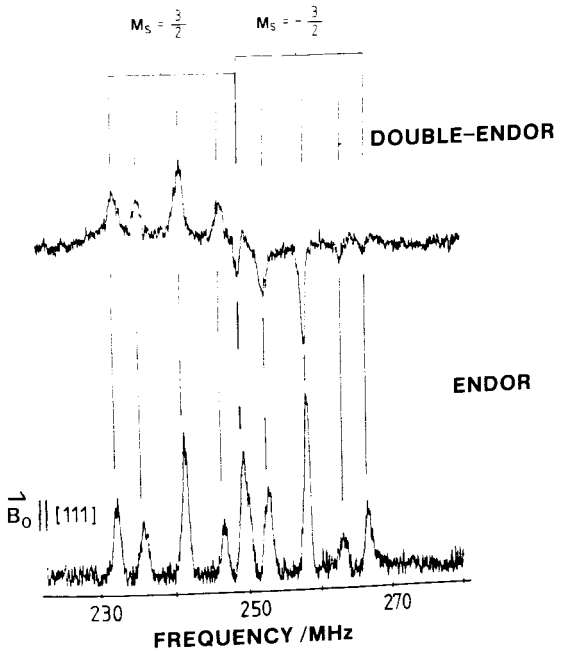

Figure 4. ENDOR and DOUBLE ENDOR spectrum of the Ga vacancy nearest-neighbor ^{31}P nuclei for $\hat{B}_0 \parallel [111]$. T = 6 K.

gether with the microwaves. One ENDOR line is chosen and its intensity is monitored as a function of the second rf frequency with a double lock-in technique. There is a signal only if both NMR transitions are indeed on nuclei belonging to the same defect, since their ENDOR transitions influence each other (16). In the stationary DOUBLE ENDOR spectrum, positive and negative signals occur, which is qualitatively understood (17, 18). Figure 4 shows the ENDOR and DOUBLE ENDOR spectra for $\hat{B}_0 \parallel [111]$. In both spectra all lines appear, proving that all lines belong to one defect. In the case of low-symmetry defects, one particular defect orientation can be selected with this method. This can be the only way to analyse unambiguously the ENDOR angular dependence, as was the case for O^- centers in α-Al_2O_3:Mg^{2+} (19).

In Figure 3 very many ENDOR lines are seen to occur, since the four nearest ^{31}P nuclei are rather strongly coupled by a pseudo-dipolar coupling. The angular dependence can be quantitatively understood by diagonalising the spin-Hamiltonian. The coupling effect resulting in rather large line splittings is bigger than reported so far (20), since the anisotropic interaction constant is

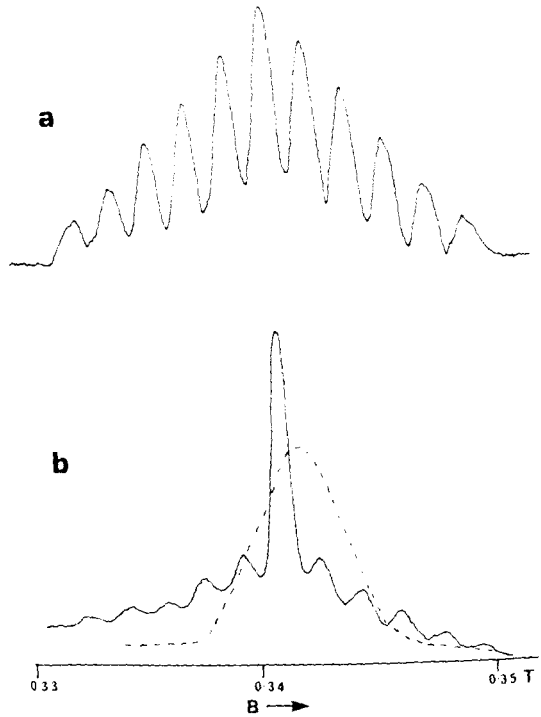

Figure 5. ENDOR-induced EPR spectra of x-irradiated (RT) Na-β-aluminate measured at several ^{27}Al ENDOR lines. (a) at 7 MHz. (b) — at 4 MHz; ---- at 13.4 MHz. Here $\hat{B}_0 \| c$-axis, T = 60 K, X-band. After (21).

very large (a/h = 195 MHz, b/h = 54.5 MHz) (J. Hage, J. R. Niklas and J.-M. Spaeth, manuscript in preparation).

A typical problem when studying radiation damage is the production of several defects and a superposition of their ENDOR spectra, which are difficult to analyse. Apart from applying the DOUBLE ENDOR technique, one can measure the ENDOR-induced EPR spectra to determine the g-factors of the EPR lines and to learn how many different defects were produced. In this technique one monitors the intensity of particular ENDOR lines as a function of the magnetic field, which is varied through the EPR lines. According to Equation [2] the ENDOR line appears only for one specific value of B_0 and varying the latter violates the double resonance condition. However, if the nuclear moment of the nucleus giving rise to the ENDOR line is known, one can maintain the double-resonance condition by synchronously varying the rf

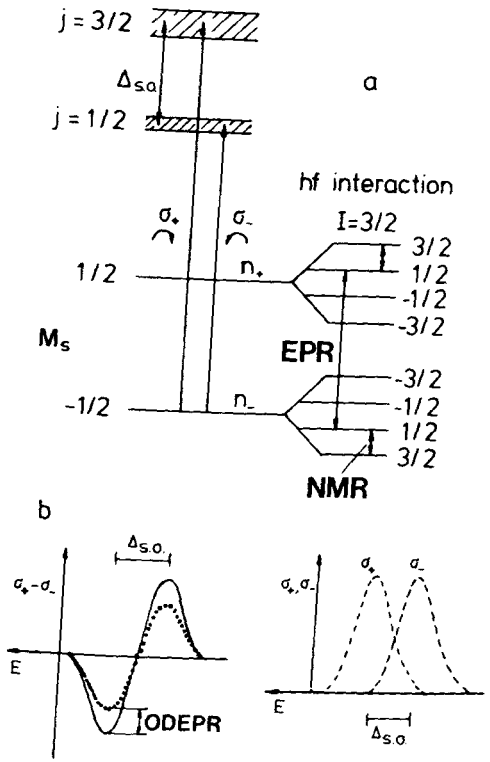

Figure 6. Schematic representation of the optical detection of the ground state EPR of a Kramers doublet *via* the microwave-induced change of the MCD of an "atomic" *s-p* transition with spin–orbit splitting in the excited state, for T = 0.

frequency with the magnetic field according to Equation [2]. One thus measures the EPR spectrum of the defect to which the particular ENDOR line belongs as a sort of excitation spectrum of the ENDOR line. Figure 5 shows as an example the ENDOR-induced EPR spectra of x-irradiated Na-β-aluminate for several ^{27}Al-ENDOR lines. Three different EPR spectra were discovered, while in the conventional EPR spectrum only the 11-line spectrum of Figure 5a is recognised. The spectrum of Figure 5a belongs to an F^+ center on a O(5) site, while those of Figure 5b belong to an F^+ center with 3 Al neighbors in the spinel block (dashed line) and to a O_2^- center in the mirror plane (central peak of solid curve) (21). ENDOR-induced EPR allows one to select spin states and to determine relative signs of spin-Hamiltonian parameters as well as to select particular defect orientations. For details, see (22, 23).

In the above, computer-aided methods for experimental control and analysis of spectra have permitted the determination of defect structures interesting for materials science. First results have been achieved in the study of small clusters like Al^{2+}-Al^{-} pairs in Si (24), Se_2^{+} pairs in Si (25) and thermal donors (oxygen clusters) in Si (26).

3. Optically Detected Electron Paramagnetic Resonance (ODEPR)

Compared to conventional EPR, optical detection has the following advantages: (i) higher sensitivity, (ii) higher selectivity, (iii) possibility of direct correlation between optical and structure properties, (iv) possibility of investigating optically excited states, (v) possibility of detecting spin-dependent non-radiative transitions, especially in semiconductors.

Some of these advantages will be illustrated for one particular technique, which recently proved to be especially useful for defect identification. The EPR of the ground state is detected as a microwave-induced change of the magnetic circular dichroism (MCD) of a defect absorption band. In Figure 6 the method is indicated schematically for an optical *s*-*p*-intracenter transition, for $T = 0$. The MCD is the difference of the absorption constant of right and left circularly polarised light. If the absorption comes from a Kramers doublet with $S = 1/2$, one obtains (3)

$$\text{MCD} = \frac{1}{2}\alpha_0 d \frac{\sigma_+ - \sigma_-}{\sigma_+ + \sigma_-} \frac{n_- - n_+}{n_- + n_+}, \tag{6}$$

where α_0 is the absorption constant of the unpolarised light, σ_+ and σ_- are the cross sections for right and left circular polarised light, respectively, n_+ and n_- are the occupation numbers for the $M_S = \pm 1/2$ states, d is the crystal thickness. If the spin–orbit splitting in the excited state is smaller than the phonon width of the absorption bands, the MCD has a derivative-like structure for $s \rightarrow p$ transitions (Figure 6). The extrema

$$\begin{aligned} \text{MCD}_{\text{extr.}} &\propto \frac{n_- - n_+}{n_- + n_+} f(\Delta_{\text{s.o.}}) \\ &\propto \tanh\left(\frac{g\beta_e B_0}{2kT}\right) f(\Delta_{\text{s.o.}}) \end{aligned} \tag{7}$$

in the intensity are proportional to the occupation difference of the Zeeman levels $\pm 1/2$ and to a function of the excited state spin–orbit interaction $\Delta_{\text{s.o.}}$. In equation [7] the so-called diamagnetic part, which is temperature indepen-

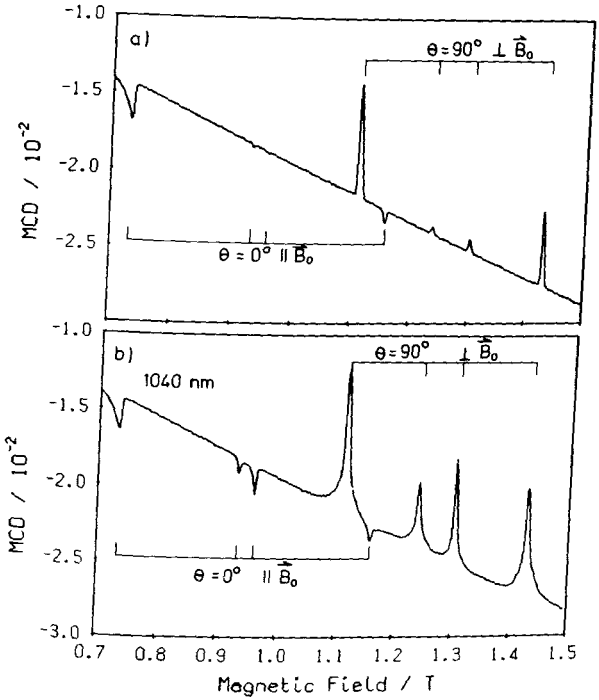

Figure 7. (a) ODEPR spectrum of $Tl^0(1)$-centers (Tl^0 atoms next to a Cl^- vacancy) in KCl detected at 1040 nm and measured at 1.5 K and 24 GHz at low microwave power (~30 db). $\theta = 0°$ ($\| \vec{B}_0$) and $\theta = 90°$ ($\perp \vec{B}_0$) refer to the orientation of the center axis (connection line Tl^0-Cl^--vacancy) relative to the magnetic field $\vec{B}_0$. (b) The same, but at higher microwave power (0 db $\hat{=}$ 500 mW). After (28).

dent, is neglected. The occupation difference of the Zeeman levels is a function of temperature and magnetic field. It is given by the well-known Brillouin-function for arbitrary S. For the simple case of $S = 1/2$, the Brillouin function reduces to essentially $\tanh(g\beta_e B_0/2kT)$. Thus, the MCD is largest for low temperatures and high magnetic field. In order to achieve a high sensitivity, one must work at low temperature. The magnetic field is determined by the EPR resonance condition (see below) and should be chosen high for searching an MCD, in case the MCD is very weak. It is favorable to place the sample into liquid helium below the λ-point ("pumped helium"), since the MCD cannot be measured with high sensitivity in boiling helium. Thus, a typical temperature for the experiment is 1.5 K. It proved also necessary to control the temperature well by controlling the helium vapor pressure. The reason is that, for ODEPR

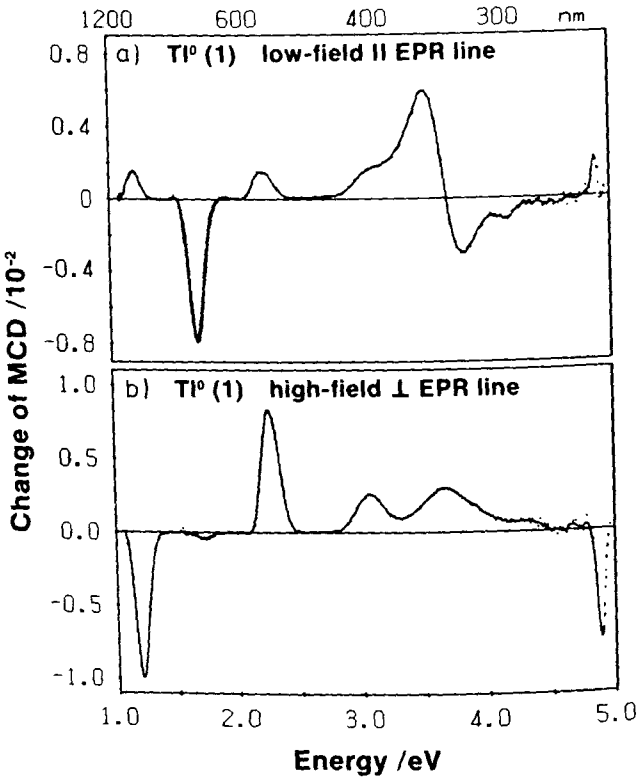

Figure 8. (a) MCD at 1.4 K of the parallel Tl^0-(1)-centers (line connecting Tl^0 and the Cl^- vacancy parallel to $\vec{B}_0$) in KCl as tagged by the corresponding low-field EPR transition. (b) The same for the perpendicular Tl^0(1) centers in KCl. After (28).

and especially for ODENDOR measurements, very small changes of the MCD have to be detected (see below). Since at low temperature the MCD is proportional to $1/T$, temperature drifts or fluctuations also cause such changes. Microwaves and radio frequency radiation have to be fed into the EPR/ENDOR cavity for the resonance experiments. The resulting power dissipation changes the vapor pressure and thus the sample temperature. This must be avoided by using a control unit.

Equation [7] holds only in the so-called rigid shift approximation, according to which the absorption bands for right and left circular polarised light are shifted by the magnetic field without resulting distortions (27). This is not the case in general. However, a quantitative understanding of the MCD is not important if one only wants to measure ODEPR or ODENDOR, since then one

uses the MCD only as the 'detection channel'.

In order to measure EPR of the ground state, microwave transitions are induced between the ground state Zeeman levels. At a given temperature and B_0, the occupation difference is reduced and therefore the reduction of $MCD_{extr.}$ can be monitored to measure EPR. Changes as small as 10^{-5} of the MCD for an optical density of 1 can be detected. If there is hf splitting, the decrease of the MCD is smaller, since only spin packets of a particular nuclear spin quantum number take part in the occupation transfer (selection rule: $\Delta M_I = 0$, $\Delta M_S = \pm 1$). Therefore, hf interactions can be resolved. Figure 7a shows the ODEPR spectrum of so-called "$Tl^0(1)$" centers in KCl. These defects have [100] axial symmetry and consist of a Tl^0 atom next to a Cl^- vacancy situated along [100]. The ODEPR spectra were measured in the lowest energy absorption band at 1040 nm. The ODEPR lines of centers located parallel and perpendicular to $\vec{B}_0$ are seen with a large Tl hf splitting ($I(^{203}Tl, ^{205}Tl) = 1/2$)); the isotope splitting is not resolved. Figure 7b shows that, with higher microwave power, forbidden transitions ($\Delta M_S = \pm 1$, $\Delta M_I = \pm 1$) occur more strongly (28). This way of measuring EPR is highly selective. If the absorption bands of several centers do not totally overlap, then each defect can be measured separately, which is not possible in conventional EPR. In order to identify all absorption transitions from one particular defect, which may be partly hidden under absorption bands of other defects simultaneously present, a kind of excitation spectroscopy of the ODEPR lines can be used. One selects a particular ODEPR transition and varies the optical wavelength while monitoring the microwave-induced change of the MCD signal. Thus, from the total MCD one measures only the part, which belongs to the particular EPR signal.

Figure 8 shows this for the $Tl^0(1)$ centers with their axes perpendicular and parallel to the magnetic field. In this way information about the polarisation of the optical transitions can also be obtained. The method of correlating optical bands with the EPR spectrum was termed "MCD tagged by EPR" (28). From the MCD bands thus measured it is however not trivial to infer the shape of the absorption bands. If the rigid shift approximation holds, then the absorption bands could be determined by integrating over the MCD. But whether it holds can only be decided if the absorption bands can be directly measured. Nonetheless, the 'tagged MCD' spectra do give valuable information about the optical absorption transitions. The approximate peak energies and band widths can be inferred and information about the transition moments (polarisation) is gained, which otherwise could not be obtained if the optical transitions are hidden under other absorption bands. A good example for this was recently

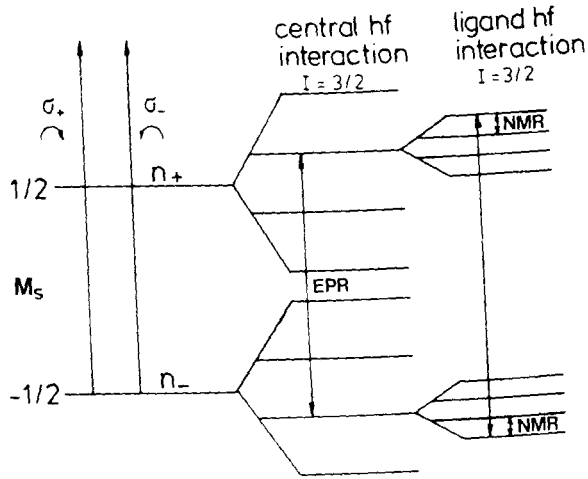

Figure 9. Schematic representation of the optical detection of ENDOR. See text.

obtained while studying the analogues of the $Tl^0(1)$ centers with Ga and In in alkali halides ($Ga^0(1)$- and $In^0(1)$-centers). Their optical bands could never have been detected otherwise since, due to a lack of fluorescence, the usual exitation spectroscopy of emission bands could not be applied and the bands were totally buried under other absorptions (29). Similarly, the optical absorption transitions associated with $[AlO_4]^0$-centers in crystalline quartz (smoky quartz) could be determined and an old question settled (30).

Another type of interesting excitation spectroscopy can be applied in semiconductors. If, *e.g.*, a deep-level defect is paramagnetic in semi-insulating material, where the Fermi level is approximately in the middle of the gap, the same defect becomes diamagnetic if by an additional doping of shallow acceptors the Fermi level is lowered to near the valence band. Then no MCD can be measured, since the defect level is empty. However if, in a double-beam experiment, electrons are excited from the valence band into the defect level, the MCD reappears. Thus, one can determine the level position relative to the valence band by measuring the photon energy for which the MCD reappears and with it the ODEPR spectrum. In this way a correlation can be established between the energy levels and the EPR spectra. This photo-ODEPR technique was recently applied for the first time. In GaAs the EPR spectrum of anion antisite defects was investigated with this method and the energy levels of two charge states of this defect could thus unambiguously be determined and correlated to the EPR lines (B. K. Meyer and J.-M. Spaeth, manuscript in preparation).

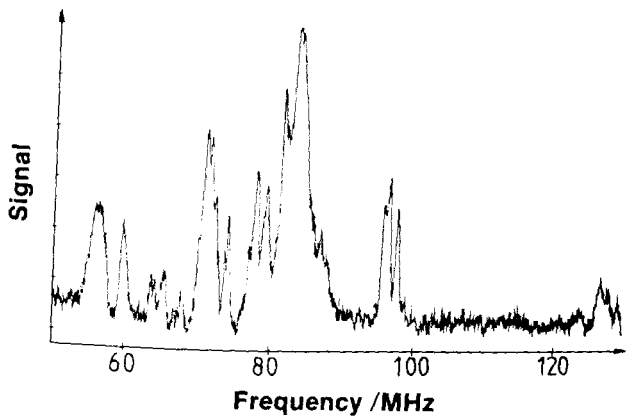

Figure 10. Section of the optically detected ENDOR spectrum of As_{Ga} defects in semi-insulating GaAs, at T = 1.5 K, with $\vec{B}_0$ in a (110) plane. The lines are due to five ^{75}As ligands.

4. Optically Detected ENDOR (ODENDOR)

The method of optical detection *via* the MCD recently proved to be very appropriate for resolving shf interactions in ENDOR. Figure 9 shows schematically the principle of this experiment for the case of one central nucleus c with $I = 3/2$ and one ligand l with $I = 3/2$ as in the case of the anion antisite defects in GaAs ($I(^{75}As) = 3/2$) in which As occupies a Ga-site (As_{Ga}). These defects were observed also with ODEPR (31). The EPR selection rule $\Delta M_l = 0$ implies, that only a fraction of the spin packets can decrease the MCD, since the microwaves induce transitions only between a particular combination of $M_{l,c}$ and $M_{l,l}$ states. If an additional NMR frequency is simultaneously applied, which combines the $M_{l,l}$ states with its neighboring ones, then more spin packets are shifted into the microwave pump channel and contribute to the decrease in MCD. Thus, with such an NMR resonance, the decrease of the MCD is enhanced, and this is monitored (32). Figure 10 shows a section of the ODENDOR spectrum of As_{Ga} defects in semi-insulating "as-grown" GaAs due to the shf interaction with five As ligands (33).

Unlike in conventional ENDOR, it was found that the ODENDOR effect is of the same order as the ODEPR effect. This is, apart from the sensitivity enhancement through the optical detection, a great advantage compared to conventional ENDOR. However, quantitatively, the size of the observed signals is not yet understood. There is yet little experience for this kind of experiment. For As_{Ga} defects in GaAs the ENDOR signal was highest when

measured in the flank of the ODEPR line, while for antisite defects in GaP the size of the ENDOR signals followed the shape of the ODEPR line. The latter would be expected from a simple hole-burning model, in analogy to conventional ENDOR. According to the latter theory, the degeneracy of the nuclear spin states, which determines the ESR line shape, should also determine the ENDOR signal heights when measuring them by varying the magnetic field through the EPR line. What happens in GaAs is not yet understood.

The ODEPR effect for As_{Ga} centers in GaAs is too great by at least one order of magnitude compared to the mechanisms discussed so far (31). The decrease of the MCD in each of the four ^{75}As hf lines is about 20%, suggestive of homogeneous EPR lines, since the total change of the MCD amounts to approximately 80%. As the ODENDOR measurements showed, however, the EPR lines are inhomogeneously broadened. There is no explanation yet for such behavior. Possibly, the dynamical nuclear polarisation of the central ^{75}As nucleus plays an important role. Altogether, more experience is needed with ODENDOR, and a theory to explain the effects observed so far needs to be developed.

Similarly, as for ODEPR, the 'MCD tagged by ENDOR' can be measured, correlating optical bands with one ENDOR line. Therefore, with this technique details of the defect structure as resolved with ENDOR can be correlated with optical properties of the defect.

More experience is available with ODENDOR in triplet state ODMR spectroscopy (34).

For a general recent review on ODMR, the reader is referred to reference (35).

Conclusion

For structure determination of point defects, the use of magnetic multiple resonance methods is very powerful. The availability of modern experimental techniques makes it possible also to tackle difficult problems interesting for materials science. The development of these methods is by no means complete. In particular the optical method can be extended further, to time-resolved measurements and to experiments where a spatial resolution of defect distribution can be measured. The increase in sensitivity can be driven further, which is of particular interest for defect studies in thin layers or interfaces.

References

1. G. FEHER. Phys. Rev. **114**, 1219, 1249 (1959).
2. B. C. CAVENETT. Adv. Phy. **30**, 475 (1981).
3. L. F. MOLLENAUER and S. PAN. Phys. Rev. B **6**, 772 (1972).
4. H. SEIDEL. Z. Phy. **165**, 218, 239 (1961).
5. C. HOENTZSCH, J. R. NIKLAS and J.-M. SPAETH. Rev. Sci. Instrum. **49**, 1100 (1978).
6. A. ABRAGAM and B. BLEANEY. Electron Paramagnetic Resonance of Transition Ions, Clarendon Press, Oxford 1970.
7. J.-M. SPAETH. *In* Defects and their Structure in Non-metallic Solids. Ed. B. Henderson and A. E. Hughes, Plenum Press, N.Y., p. 155, 1976.
8. Y. UEDA, J. R. NIKLAS, J.-M. SPAETH, U. KAUFMANN and J. SCHNEIDER. Solid State Commun. **46**, 127 (1983).
9. J. R. NIKLAS. Habilitationsschrift, Paderborn, 1983.
10. M. U. A. BROMBA and H. ZIEGLER. Anal. Chem. **51**, 1760 (1979).
11. H. ZIEGLER. Appl. Spectr. **35**, 88 (1981).
12. M. U. A. BROMBA and H. ZIEGLER. Anal. Chem. **55**, 648 (1983).
13. M. U. A. BROMBA and H. ZIEGLER. Anal. Chem. **56**, 2052 (1984).
14. S. GREULICH-WEBER, J. R. NIKLAS, E. WEBER and J.-M. SPAETH. Phys. Rev. B **30**, 6292 (1984).
15. J. HAGE, J. R. NIKLAS and J.-M. SPAETH. Phys. Verhandl. DPG (VI), **21**, 1093 (1986).
16. R. BIEHL, M. PLATO and K. MÖBIUS. J. Chem. Phys. **63**, 3515 (1975).
17. N. S. DALAL and C. A. MCDOWELL. Chem. Phys. Letts. **6**, 617, (1970).
18. J. R. NIKLAS, R. U. BAUER and J.-M. SPAETH. Phys. Status Solidi (b) **119**, 171 (1983).
19. R. C. DUVARNEY, J. R. NIKLAS and J.-M. SPAETH. Phys. Status Solidi (b) **128**, 673 (1985).
20. T. E. FEUCHTWANG. Phys. Rev. **126**, 1628 (1962).
21. R. C. BARKLIE, J. R. NIKLAS and J.-M. SPAETH. J. Phys., Colloq. **41**, C6-537 (1980).
22. J. R. NIKLAS and J.-M. SPAETH. Phys. Status Solidi (b) **101**, 221 (1980).
23. J.-M. SPAETH and J. R. NIKLAS. Recent Developments in Condensed Matter Physics, **1**, 393 (1981).
24. J. R. NIKLAS, J.-M. SPAETH and G. D. WATKINS. Mater. Res. Soc. Symp. Proc. **46**, 237 (1985).
25. S. GREULICH-WEBER, J. R. NIKLAS and J.-M. SPAETH. Verhandl. DPR (VI), **21**, 1092 (1986).
26. J. MICHEL, J. R. NIKLAS and J.-M. SPAETH. MRS Symp. Proc. Fall 1985, Boston (1986).
27. C. H. HENRY and C. P. SLICHTER. *In* Physics of Color Centers, Ch. 6, Ed. by W. B. Fowler. Acad. Press, N.Y. (1968).
28. F. J. AHLERS, F. LOHSE, J.-M. SPAETH and L. F. MOLLENAUER. Phys. Rev. B **28**, 1249 (1983).
29. F. J. AHLERS, F. LOHSE, T. HANGLEITER, J.-M. SPAETH and R. H. BARTRAM. J. Phys. C **17**, 4877 (1984).
30. B. K. MEYER, F. LOHSE, J.-M. SPAETH and J. A. WEIL. J. Phys. C **17**, L31 (1984).
31. B. K. MEYER, J.-M. SPAETH and M. SCHEFFLER. Phys. Rev. Letts. **52**, 851 (1984).
32. D. M. HOFMANN, B. K. MEYER, F. LOHSE and J.-M. SPAETH. Phys. Rev. Letts. **53**, 1187 (1984).
33. J.-M. SPAETH. Proc. of the 4th Int. Conf. on Semi-insulat. III-V Materials, Hakone, Japan, 1986.
34. K. P. DINSE and C. J. WINSCON. 'Optically-detected ENDOR Spectroscopy' *In* Triplet State ODMR Spectroscopy, Ed. R. H. Clarke, John Wiley, N.Y. 1984.
35. W. B. LYNCH and D. W. PRATT. Magn. Reson. Rev. **10**, 111 (1985).